Journal of Energy Chemistry 49 (2020) 174–178

Contents lists available at ScienceDirect

Journal of Energy Chemistry

journal homepage: www.elsevier.com/locate/jechem

http://www.journals.elsevier.com/journal-of-energy-chemistry/

Communication

A laser synthesis of vanadium oxide bonded graphene for high-rate supercapacitors

Jun Tang[a,b], Linfei Zhang[b], Xiongwei Zhong[b], Xinghui Wang[c], Feng Pan[a,*], Baomin Xu[b,*]

[a] School of Advanced Materials, Peking University Shenzhen Graduate School, Peking University, Shenzhen 518055, Guangdong, China
[b] Department of Materials Science and Engineering, Southern University of Science and Technology, Shenzhen 518055, Guangdong, China
[c] Institute of Micro/Nano Devices and Solar Cells, School of Physics and Information Engineering, Fuzhou University, Fuzhou 350108, Fujian, China

ARTICLE INFO

Article history:
Received 27 December 2019
Revised 3 February 2020
Accepted 4 February 2020
Available online 24 February 2020

Keywords:
Supercapacitors
Restacking
Vanadium oxides
Laser reduced graphene
High rate

ABSTRACT

Graphene is a type of promising electrode material for high-energy and high-power density supercapacitors, but its electrochemical performance is greatly limited by the restacking problem. In this work, we reported a facile approach to synthesis graphene with chemically bonded vanadium oxide (VO_x) nanoparticles and demonstrated that chemically-bonded VO_x nanoparticles can effectively prevent the graphene sheets from restacking and hence improve the electrochemical performance. The capacitance of VO_x-bonded graphene increases to 272 F/g compared to 183 F/g of pristine graphene in 1 M H_3PO_4 aqueous electrolyte at 2 A/g. The VO_x-bonded graphene also showed improved rate capability in both H_3PO_4 and ionic liquid electrolytes. The capacitance retention increases to 54.5% from 28.5% at 100 A/g (compare to 2 A/g) in H_3PO_4 and increases to 65.1% from 46.3% at 2 A/g (compare to 0.2 A/g) in neat ionic liquid. A high energy density of 84.4 Wh/kg is obtained within the voltage window of 4 V in ionic liquid. Even at a high-power density of 1000 W/kg, the VO_x-bonded graphene shows a high energy density of 47.3 Wh/kg.

Supercapacitors have been intensively studied as electrochemical energy storage devices due to their ultrafast charge/discharge capability and ultra-long cycle life [1–6]. As a type of most widely commercialized supercapacitors, electrical double layer capacitors (EDLCs), which store/deliver electrical energy via physical adsorption/desorption of electrolyte ions on the electrode/electrolyte interfaces, show outstanding fast energy storage/delivery performance [7–10]. However, due to the mechanism of surface energy storage, EDLCs exhibit ultra-low energy density. Increasing the operate voltage window is an effective way to increase the energy density of EDLCs by using organic/ionic liquid electrolytes, according to the relationship of $E = 1/2\ CV^2$, where E is the energy density, C is the capacitance and V is the working voltage window. However, the power density will decrease dramatically when organic/ionic liquid electrolytes are used due to the low ion conductivity and large ion size of the electrolyte ions [11,12]. As a result, the application of EDLCs has been greatly limited since in most of the energy storage applications, both high-energy and high-power density are required. This problem can be solved by either increase the capacitance in aqueous electrolytes or improve the rate performance in organic/ionic liquid electrolytes.

Graphene is a promising candidate for high-energy and high-power density supercapacitors because of its high surface area (high capacitance, contributing to energy density) and good conductivity (high rate performance, contributing to power density) [13–17]. The intrinsic capacitance of single-layer graphene was reported to be ~21 $\mu F/cm^2$ and the theoretical maximum capacitance for EDLC based on graphene materials could, in principle, reach ~550 F/g if the entire surface area can be used [18]. However, the current practical graphene-based capacitances are generally lower than 100 F/g due to the restacking problem [19–24]. The 2D graphene oxide (GO)/graphene sheets can easily stack together and overlap, which results in the loss of effective surface area and hinders the vertical ion transportation. Both the capacitance and the rate capability of graphene electrode are limited by the restacking problem, which results in low energy and low power density. There are various ways in solving the restacking problem of graphene film [25,26]. Luo et al. showed that the capacitance of restacked graphene was as low as 36 F/g when charged/discharged at a current density of 2 A/g in aqueous potassium hydroxide [27]. They successfully synthesized crumpled graphene balls to alleviate the restacking problem and achieved a much higher capacitance of 118 F/g at the same current density. El-Kady developed a facile laser reduction method and achieved a much higher capacitance value of 202 F/g in H_3PO_4 aqueous electrolyte at 1 A/g

* Corresponding authors.
E-mail addresses: panfeng@pkusz.edu.cn (F. Pan), xubm@sustech.edu.cn (B. Xu).

https://doi.org/10.1016/j.jechem.2020.02.015

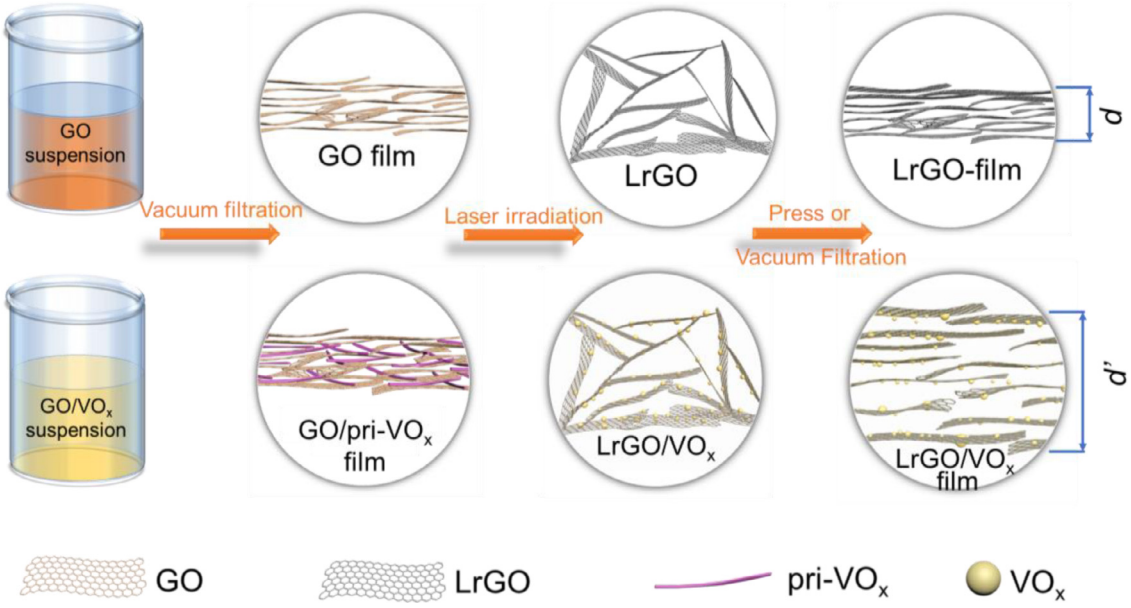

Fig. 1. Schematic illustration of laser reduced graphene and VO_x bonded graphene processes.

[28]. Kaner's work demonstrated that the GO film can be expanded by laser irradiation, which converts the restacked GO sheets immediately into well-exfoliated few-layered grapheme film, resulting in high capacitance. Luo's and El-Kady's works represent two typical strategies in solving the restacking problem of graphene sheets, which could be concluded as unstacking treatments pre- and post-GO/graphene film forming (pretreatment and posttreatment) method, respectively. Various works, afterwards, have further proved and demonstrated the effectiveness of pretreatment or posttreatment methods [26,29–32]. However, the curved nature of graphene by Luo's method and the expansion of graphene by El-Kady's laser method will largely decrease the volumetric energy density. Direct press of the curved/expanded graphene can directly increase the volumetric energy density but will cause the restacking problem again [33].

Herein, we integrated both pretreatment and posttreatment methods for the first time to further solve the restacking problem. In this work, we showed that pristine vanadium oxide (pri-VO_x) nanofibers inserted between GO sheets can protect GO film from restacking together. Afterward, pri-VO_x nanofibers were laser converted into nanoparticles which are chemically bonded to the graphene surface. Synchronously, the separated GO sheets were further laser exfoliated and reduced. Accordingly, VO_x nanoparticles effectively prevent the graphene sheets from restacking when press or vacuum filtrate the loose reduced graphene into film again and thus improved the electrochemical performances. Specifically, both the capacitances in aqueous electrolytes and the rate performance in ionic liquid electrolytes were improved significantly and thereby, both high-energy and high-power density were obtained.

Graphene free-standing films are usually used directly as electrodes for various energy storage devices. In a typical synthesis process, GO sheets are vacuum filtrated into free-standing films and then chemically, thermally or laser reduced into graphene films. Fig. 1 shows a typical synthesis process of graphene films using laser reduction method. The GO sheets will stack together easily during the vacuum filtration process. Laser irradiation can simultaneously convert GO into graphene and exfoliate graphene sheets to a certain extent. The loose laser reduced graphene oxide (LrGO) can be directly pressed or re-dispersed and re-vacuum filtrated into films. However, the LrGO film will restack again and the performance will decrese accordingly. To further unstack the graphene sheets, pri-VO_x nanofibers are pre-inserted into GO interlayer space as a pretreatment method to prevent GO sheets from restacking. The pri-VO_x nanofibers can be converted into nano particles (containing V_2O_5 and VO_2, Fig. S2) that chemically bonded to the graphene sheet during the laser irradiation process. When directly pressed or re-dispersed and re-vacuum filtrated into films, the VO_x nanoparticles can keep the interlayer space between adjacent graphene layers. By using this combined pretreatment and posttreatment method, highly unstacked graphene film was obtained.

It can be seen that the GO sheets are well seperated by pri-VO_x nanofibers by comparing Fig. 2(a and c). The GO/pri-VO_x film shows clear layered edges, indicating the loose stacked nature of the film (compare the inset images of Fig. 2a and c). The GO/pri-VO_x film also shows increased interlayer space (Fig. 2e) because of the intercalation of pri-VO_x nanofibers. After laser reduction, the GO film pre-intercalated with pri-VO_x nanofibers (LrGO/VO_x) becomes more loose stacked (Fig. 2d) than LrGO (Fig. 2a) and shows even higher specific surface area than LrGO (Fig. S3). The pri-VO_x nanofibers are laser converted into ~5 nm particles on graphene sheet (inset of Fig. 2d), which are both horizontally and vertically distributed in the LrGO/VO_x film uniformly (Fig. S4). During the laser irradiation process, the GO sheets are reduced into graphene with the removal of large amount of C–O bonds (Fig. 2f and g). Surprisingly, a new peak appears at a binding energy of 530.4 eV, which can be assigned to the V-O-C bond, indicating that VO_x nanoparticles are chemically bonded to the graphene sheets.

When pressed into film, the higher SSA and larger interlayer space of LrGO/VO_x can be retained and accordingly, will contributed to higher capacitance (Fig. 3a). The capacitance of LrGO/VO_x was compared to the reported capacitances of graphene reduced by various techniques (Table S1). The LrGO/VO_x showed a high capacitance of 272.6 F/g at a current density of 2 A/g with relatively high areal mass loading of 1.2 mg/cm^2. This capacitance seems to be among the highest values of reported reduced graphene oxide supercapacitors. Moreover, LrGO/VO_x film also shows higher rate performance (Fig. 3b). When charged/discharged at a very high current density of 100 A/g, 54.5% of the initial capacitance at 2 A/g can be retained for LrGO/VO_x film. While only 28.5% of the initial capacitance can be retained for the LrGO film. The LrGO/VO_x film also shows excellent cycling performance and

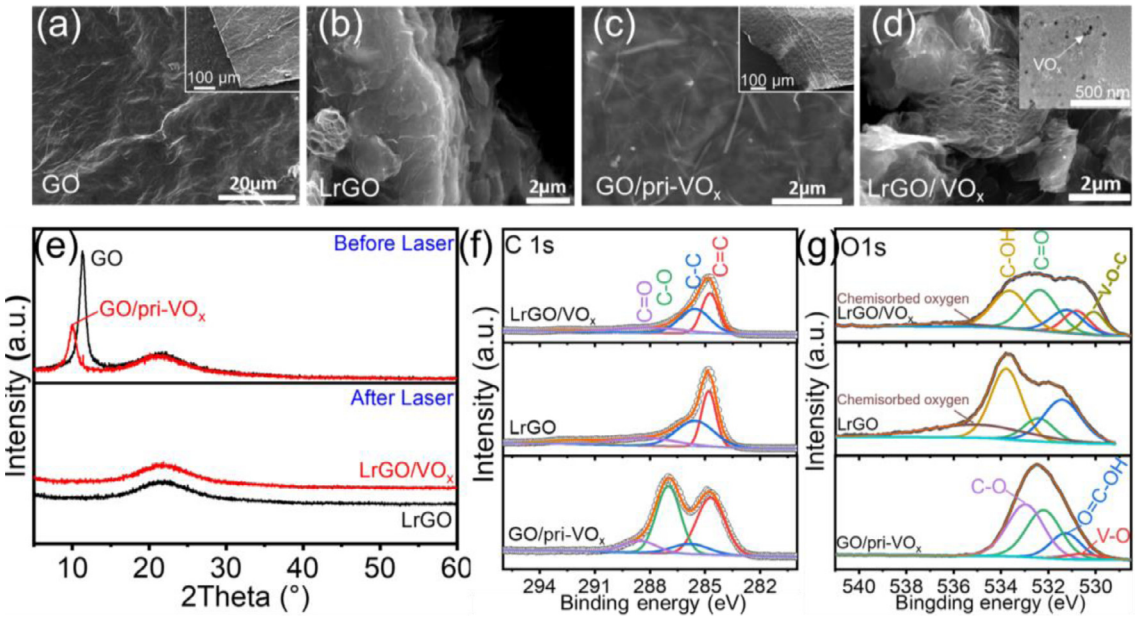

Fig. 2. Morphology and structure changes after laser irradiation. Scanning electron microscopy (SEM) images of GO (a) before and (b) after laser reduction; SEM images of GO/pri-VO_x (c) before and (d) after laser irradiation; (e) X-ray diffraction (XRD) and (f,g) X-ray photoelectron spectroscopy (XPS) of GO and GO/pri-VO_x before and after laser treatment.

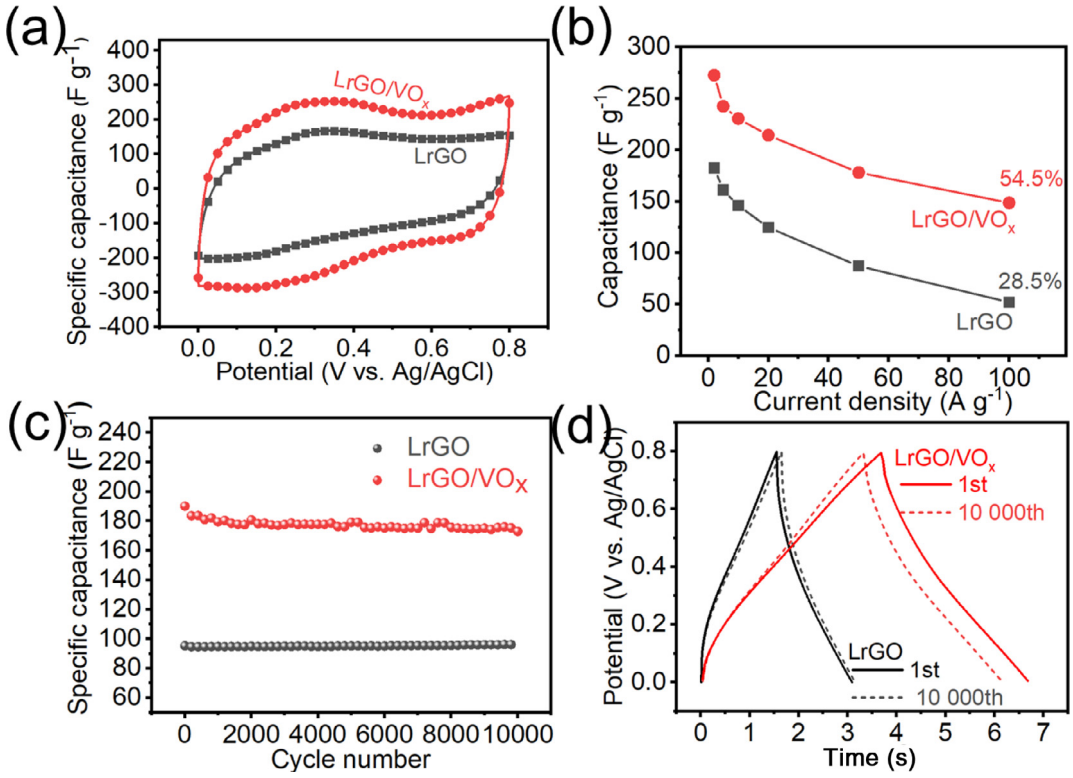

Fig. 3. Electrochemical performance in 1 M H_3PO_4 aqueous electrolyte. (a) Cyclic voltammetry (CV) curves of LrGO and LrGO/VO_x at a scan rate of 100 mV/s. (b) Rate performance comparison of LrGO and LrGO/VO_x at different current densities. (c) Cycle performance of LrGO and LrGO/VO_x. (d) Charge/discharge curves of LrGO and LrGO/VO_x before and after cycle performance test.

>90% of the capacitance can be retained after 10,000 cycles (Fig. 3c). By comparing the charge/discharge curve before and after cycle (Fig. 3d), it can be seen that the capacitance loss comes mainly from the high potential range for LrGO/VO_x, which may be ascribed to the capacitance loss of the VO_x nanoparticles. According to Fig. 3(d), the Coulombic efficiencies for LrGO before and after cycle are 90.9% and 99.4%, respectively and for LrGO/VO_x, the efficiencies are 82.4% and 85.4%, respectively. The low Coulombic efficiency of LrGO/VO_x can be ascribed to the water split catalyzed by VO_x since a significant increase in current density was observed around 0.8 V from the CV curve of the bare VO_x (Fig. S7b, Supporting Information). To better understand the electrochemical behavior, the electrochemical performance of bare-VO_x was tested as shown in Fig. S7(a). The bare VO_x shows a capacitance as low as 39 F/g, which is

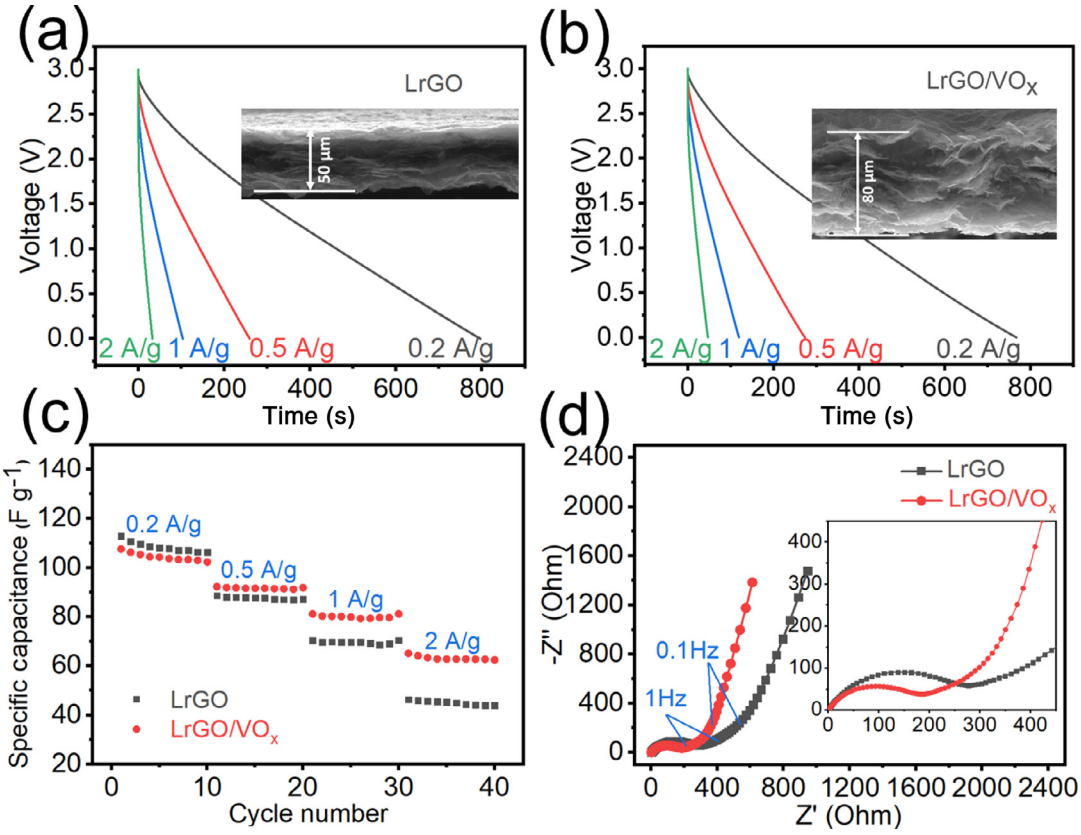

Fig. 4. Electrochemical performance in ion liquid electrolyte. Charge/discharge curves of (a) LrGO and (b) LrGO/VO_x coin cells in EMI-BF_4 ionic liquid electrolyte within a voltage window of 3 V. (c) Rate performance of LrGO and LrGO/VO_x within a voltage window of 3 V. (d) EIS at 0 V of LrGO and LrGO/VO_x coin cells after rate performance test.

much lower than that of LrGO. After cycled at 50 A/g in 1 M H_3PO_4 electrolyte for 1.5 h (corresponding to the time used for the first 1000 cycles of LrGO/VO_x, the capacitance of bare VO_x decreased to 21 F/g (~54% remained, nearly half lost and half remained). Therefore, assuming the capacitance fading of LrGO/VO_x at the first 1000 cycles (~9%) is ascribed to the capacitance loss of VO_x and thus the capacitance contribution of VO_x in LrGO/VO_x after 1000 cycles can be roughly calculated to be ~10%. However, the capacitance of LrGO/VO_x is ~80% higher than LrGO at after 1000 cycles, indicating that the capacitance contribution from VO_x is limited and can be negligible.

Symmetric LrGO and LrGO/VO_x coin cells were assembled to test the electrochemical performance in EMI-BF_4 ionic liquid electrolyte. The discharge curves of LrGO and LrGO/VO_x are shown in Fig. 4(a and b), respectively. The LrGO shows a slightly higher capacitance than that of LrGO/VO_x at a low current density of 0.2 A/g. The capacitance difference is only 3.5%, which may be resulted from the inactive mass content of VO_x in LrGO/VO_x (~3.7 wt%, Fig. S1). The LrGO/VO_x with enlarged interlayer space (insets of Fig. 4a and b) shows higher rate performance (Fig. 4c). The capacitance retention increases from 46.3% to 65.1% when the charge/discharge current density increases from 0.2 to 2 A/g within a voltage window of 3 V. The higher rate performance of LrGO/VO_x calculated from the discharge curves showed consistency with the CV results shown in Fig. S8, where larger CV area was obtained for LrGO/VO_x. The 4 V performance has also been tested and is shown in Fig. S9, which also displays a rate capability increase. The high rate performance may be ascribed to the increased surface areaand the decreased resistance at lower frequencies (Figs. 4d and S9d). The increased rate capability may be also attributed to the loose stacked structure of LrGO/VO_x (the inset SEM images in Fig. 4a and b) where VO_x works as spacer between LrGO sheets and thus electrolyte ions can transport faster. As shown in Fig. S11, the 4 V voltage window allows the LrGO/VO_x to achieve a high energy density of 84.4 Wh/kg at 0.5 A/g. Even at a high power density of 1000 W/kg, the LrGO/VO_x shows a high energy density of 47.3 Wh/kg. Fig. 4(d) shows that the impedence values at 10^5 Hz are almost the same for both supercapacitors, indicating the inner resistance of graphene has not been significantly changed by VO_x. However, the semi-circle diameter of the EIS spectra of LrGO/VO_x supercapacitor at high frequences are smaller and the slope at lower frequences are larger than LrGO supercapacitor, which implies that both the charge transfer and diffusion resistance resistances are smaller for LrGO/VO_x supercapacitor compared to LrGO supercapacitor.

In conclusion, pre-inserted pri-VO_x nanofibers can effectively prevent the GO sheets from restacking together. Laser reduction is an effective method for restacked GO film reduction and exfoliating. By combining these two methods, the GO sheets pre-exfoliated by pri-VO_x inserting can be further exfoliated by laser irradiation and highly unstacked graphene can be obtained. Consequently, ultrahigh capacitance of 272.6 F/g of the graphene is obtained in 1 M H_3PO_4 electrolyte. This value is among the highest values that have been reported in graphene-based supercapacitors using aqueous electrolytes. An improved rate performance has also been obtained in neat ionic liquid electrolyte for the VO_x-bonded graphene.

Declaration of Competing Interest

The authors declare that they have no known competing financial interests or personal relationships that could have appeared to influence the work reported in this paper.

Acknowledgments

This work is supported by the Fundamental Research (Discipline Arrangement) Project funding from Shenzhen Science and Technology Innovation Committee (Grant no. JCYJ20170412154554048), the Peacock Team Project funding from Shenzhen Science and Technology Innovation Committee (Grant no. KQTD2015033110182370), and the National Key Research and Development Project funding from the Ministry of Science and Technology of China (Grants nos. 2016YFA0202400 and 2016YFA0202404), the Shenzhen Maker Project for Students (Grant no. GRCK2017042410565958), the Guangdong Innovation Team Project (no. 2013N080), and the Shenzhen Peacock Plan (Grant no. KYPT20141016105435850).

Supplementary materials

Supplementary material associated with this article can be found, in the online version, at doi:10.1016/j.jechem.2020.02.015.

References

[1] L.L. Zhang, X.S. Zhao, Chem. Soc. Rev. 38 (2009) 2520–2531.
[2] Y. Shao, M.F. El-Kady, L.J. Wang, Q. Zhang, Y. Li, H. Wang, M.F. Mousavi, R.B. Kaner, Chem. Soc. Rev. 44 (2015) 3639–3665.
[3] P. Simon, Y. Gogotsi, Nat. Mater. 7 (2008) 845–854.
[4] B. Jiang, X. Ban, Q. Wang, K. Cheng, K. Zhu, K. Ye, G. Wang, D. Cao, J. Yan, J. Mater. Chem. A 7 (2019) 24374–24388.
[5] J. Yang, X. Xiao, P. Chen, K. Zhu, K. Cheng, K. Ye, G. Wang, D. Cao, J. Yan, Nano Energy 58 (2019) 455–465.
[6] H. Niu, X. Yang, Q. Wang, X. Jing, K. Cheng, K. Zhu, K. Ye, G. Wang, D. Cao, J. Yan, J. Energy Chem. 46 (2020) 105–113.
[7] H. Jiang, P.S. Lee, C. Li, Energy Environ. Sci. 6 (2013) 41–53.
[8] E. Raymundo-Pinero, F. Leroux, F. Beguin, Adv. Mater. 18 (2006) 1877–1882.
[9] G. Wang, L. Zhang, J. Zhang, Chem. Soc. Rev. 41 (2012) 797–828.
[10] E. Frackowiak, Phys. Chem. Chem. Phys. 9 (2007) 1774–1785.
[11] F. Béguin, V. Presser, A. Balducci, E. Frackowiak, Adv. Mater. 26 (2014) 2219–2251.
[12] K.L. Van Aken, M. Beidaghi, Y. Gogotsi, Angew. Chem. Int. Ed. 54 (2015) 4806–4809.
[13] Z. Yang, W. Zhao, Y. Niu, Y. Zhang, L. Wang, W. Zhang, Q. Li, Carbon 132 (2018) 241–248.
[14] Z. Song, W. Li, Y. Bao, Z. Sun, L. Gao, M.H. Nawaz, D. Han, L. Niu, Carbon 136 (2018) 46–53.
[15] S. Kannappan, H. Yang, K. Kaliyappan, R.K. Manian, A.S. Pandian, Y.S. Lee, J.H. Jang, W. Lu, Carbon 134 (2018) 326–333.
[16] P. Xu, Q. Gao, L. Ma, Z. Li, H. Zhang, H. Xiao, X. Liang, T. Zhang, X. Tian, C. Liu, Carbon 149 (2019) 452–461.
[17] Z. Yang, J. Tian, Z. Yin, C. Cui, W. Qian, F. Wei, Carbon 141 (2019) 467–480.
[18] J. Xia, F. Chen, J. Li, N. Tao, Nat. Nanotechnol. 4 (2009) 505–509.
[19] J. Li, J. Tang, J. Yuan, K. Zhang, Y. Sun, H. Zhang, L.C. Qin, Electrochim. Acta 258 (2017) 1053–1058.
[20] W. Ma, S. Chen, S. Yang, W. Chen, W. Weng, Y. Cheng, M. Zhu, Carbon 113 (2017) 151–158.
[21] A. Ramadoss, K.Y. Yoon, M.-J. Kwak, S.I. Kim, S.-T. Ryu, J.-H. Jang, J. Power Sources 337 (2017) 159–165.
[22] H. Yang, S. Kannappan, A.S. Pandian, J.H. Jang, Y.S. Lee, W. Lu, Nanotechnology 28 (2017) 445401.
[23] S. Subramanian, M.A. Johny, M.M. Neelanchery, S. Ansari, Power Electron. (2018) 1-1.
[24] B. Wang, Y. Qin, W. Tan, Y. Tao, Y. Kong, Electrochim. Acta 241 (2017) 1–9.
[25] C. Liu, Z. Yu, D. Neff, A. Zhamu, B.Z. Jang, Nano Lett. 10 (2010) 4863–4868.
[26] X. Yang, C. Cheng, Y. Wang, L. Qiu, D. Li, Science 341 (2013) 534–537.
[27] J. Luo, H.D. Jang, J. Huang, ACS Nano 7 (2013) 1464–1471.
[28] M.F. El-Kady, V. Strong, S. Dubin, R.B. Kaner, Science 335 (2012) 1326–1330.
[29] Q. Yang, S.K. Pang, K.C. Yung, J. Power Sources 311 (2016) 144–152.
[30] J.H. Lee, N. Park, B.G. Kim, D.S. Jung, K. Im, J. Hur, J.W. Choi, ACS Nano 7 (2013) 9366–9374.
[31] M.Q. Zhao, Q. Zhang, J.Q. Huang, G.L. Tian, J.Q. Nie, H.J. Peng, F. Wei, Nat. Commun. 5 (2014) 3410.
[32] C. Liu, Z. Yu, D. Neff, A. Zhamu, B.Z. Jang, Nano Lett. 10 (2010) 4863–4868.
[33] P. Lv, X. Tang, R. Zheng, X. Ma, K. Yu, W. Wei, Nanoscale Res. Lett. 12 (2017) 630–640.